Materials Advances

ROYAL SOCIETY OF CHEMISTRY

PAPER

View Article Online
View Journal | View Issue

Cite this: *Mater. Adv.*, 2026, 7, 874

Controlling the phase transition dynamics of GeTe by Sn substitution for phase change memory, photodetection and neuromorphic devices

Mubaris N. K.,[a] Rajkumar Shanajaoba Singh,[a] Prabhukrupa Chinmay Kumar,[b] Ramakanta Naik[b] and Vinod E. Madhavan*[a]

Chalcogenide-based phase change memories are considered for next-generation phase change random access memory (PCRAM) applications because of their unique reversible crystallization and amorphization properties. This study investigates the effects of substituting germanium (Ge) with tin (Sn) in GeTe-based phase-change memory (PCM) materials. Substitution with Sn can play a crucial role because it decreases the electrical bandgap and lowers the phase transition temperature, which benefits tailored low-power PCM and neuromorphic applications. The addition of Sn accelerates the crystallization process to the stable cubic phase, potentially controlling the PCM device's switching speed. Furthermore, optimizing the Ge/Sn ratio is crucial, as excessive Sn may lead to enhanced resistance contrast and reduced data retention, and can be utilized in applications such as multi-bit memory devices. Although both alloys can be used for memory applications due to their distinct phase contrast, the presence of Sn replacing Ge appears to be an ideal choice for photosensor applications as well. The photoresponse study of the prepared samples under dark and light conditions assessed the photodetection ability of the materials. Annealing played a crucial role in enhancing the photodetection performance of the prepared films, leading to a sustainable alternative for photodetection devices using chalcogenide semiconductor materials. These findings contribute to the development of more tunable and reliable PCM materials for future memory and photosensor applications. The potential of bandgap engineering and tuning transition temperature reveals the importance of lowering the impulses for neuromorphic applications.

Received 4th September 2025,
Accepted 27th November 2025

DOI: 10.1039/d5ma01008j

rsc.li/materials-advances

I. Introduction

The advent of phase change material (PCM) based nonvolatile memory products has revolutionized the computing landscape, effectively bridging the performance gap between solid-state drives (SSDs) and dynamic random-access memory (DRAM).[1] Moreover, these innovative memory cells can be configured into neural network-like architectures *via* crossbar arrays, enabling direct arithmetic computations, logical operations, and even machine learning tasks within memory units.[2] This paradigm, dubbed neuro-inspired computing, promises unparalleled efficiency in power consumption and computational prowess, primarily by obviating the need for extensive data transfer between disparate processing and memory units[1–6]

When chalcogenide PCMs transform from amorphous to crystalline (abbreviated as a–c phase transition), their electrical properties will change from high resistance to low resistance. The a–c phase transition of PCMs is characterized by fast switching speed, non-volatility, and reversibility.[7,8] PCM-based memory cells can be assembled into devices that have more efficient storage applications, fast transition speeds, non-volatility, and thermal stability. And hence, massive and extensive data transfer between multiple memory cells can be done. Here, the crystallization and amorphization correspond to SET and RESET operations, respectively. The large contrast in electrical resistance is used to identify the binary logic states "0" (high resistance amorphous state) and "1" (low resistance crystalline state). The bottleneck in phase change materials in memory applications was also addressed by the cell architecture design to reduce the programming current and hence RESET power.[9–11]

The well-known PCM material $Ge_2Sb_2Te_5$ (GST) lies in the GeTe–Sb_2Te_3 pseudo-binary tie-line, where one end of the

[a] *Semiconductor and Optoelectronics Lab, Department of Materials Science and Engineering, National Institute of Technology Calicut, Kozhikode, Kerala 673601, India. E-mail: vinodem@nitc.ac.in, mubaris_p240562mt@nitc.ac.in, rajkumar_p240165mt@nitc.ac.in*

[b] *Department of Engineering and Materials Physics, Institute of Chemical Technology-Indian Oil Odisha Campus, Bhubaneswar, Odisha 751013, India. E-mail: prabhumohanty128@gmail.com, ramakanta.naik@gmail.com*

tie-line is GeTe material.[12–14] Due to the need for cost-effectiveness in commercial applications, researchers continue to search for the best phase change memory materials. To do this, several studies have investigated, replacing the expensive metal Germanium with less expensive substitutes, opening the door for PCM technology to be widely employed.[4] For doping the elements having a large atomic radius, doped atoms tend to replace the matrix atoms and bond with each other to optimize the phase change performance.[2,8,15] Since Sn and Ge are in the same group (14), they possess the same number of outer electrons and atomic structures, hence having similar properties.[16–18] Most research has reported that Sn doping can tune the phase transition speed and reduce the melting point.[19–22] Another study pointed out that Sn incorporation makes distortions in the GeTe lattice and forms a more stable cubic structure, while the lattice parameters have increased due to the larger atomic radius of Sn atoms compared to Ge atoms.[20]

Resistance drift, a process characterized by the gradual increase in electrical resistance of the amorphous phase, presents issues for the stability of phase change materials (PCM). Research indicates that replacing Ge with Sn significantly mitigates this drift, resulting in enhanced memory stability.[4] *Ab initio* simulations demonstrate that elevated Sn content diminishes the prevalence of tetrahedral motifs and the extent of Peierls distortion in amorphous GeTe.[23] This reduction correlates with diminished resistance drift, attributed to the enhanced ionicity resulting from the substitution of Ge with Sn. This substitution affects various properties critical to PCM performance and neuro-inspired computing. Experimental studies have explored the effects of substituting Ge (germanium) with Sn (tin) in GeTe-based phase-change memory (PCM) materials, revealing notable changes in their properties. In this study, we are exploring the possibilities of substituting Ge with 50% of Sn to study compositional dependent changes. To elucidate the phase transition behavior of Sn-doped GeTe, a systematic study was undertaken, wherein samples of $Ge_{1-x}Sn_xTe$ with $x = 0$ (GeTe) and 0.5 ($Ge_{0.5}Sn_{0.5}Te$-abbreviated as GeSnTe) were synthesized and characterized.

The photoresponse study of GeTe and GeSnTe thin film samples was conducted to understand photoresponsivity and other critical parameters, such as responsivity and detectivity. The photoresponse of GeTe and GeSnTe thin films plays a pivotal role in determining their potential for optoelectronic and photonic applications. These materials exhibit tunable bandgaps and strong absorption in the near-infrared to visible regions, making them suitable for photodetectors, infrared sensors, and memory devices. GeSnTe, in particular, benefits from the incorporation of Sn, which modifies the electronic structure and can enhance carrier mobility and photoresponsivity. The pronounced photoresponse arises from the strong spin–orbit coupling and phase-change behavior inherent to these chalcogenides, enabling fast and reversible changes in optical and electrical properties under light exposure. Understanding and optimizing the photoresponse characteristics of these films is essential for advancing their integration into next-generation non-volatile memories, reconfigurable photonic circuits, and neuromorphic computing platforms.

II. Experiments

a. Sample preparation and characterization techniques

Highly pure Ge (99.999%, Unique Metals), Te (99.8%, Sigma Aldrich), and Sn (99.8%, Sigma Aldrich) were measured in stoichiometric proportions and sealed under vacuum ($\sim 1 \times 10^{-5}$ mbar) in glass ampoules. The bulk materials were synthesized using the melt-fusing technique in a high-temperature furnace. The sealed ampoules underwent heating at 5 °C min^{-1} up to 950 °C, were maintained for 12 hours, followed by natural cooling to ambient temperature. Thin films were subsequently produced from the bulk samples *via* thermal evaporation using molybdenum boats. The deposition chamber was maintained at $\sim 2 \times 10^{-5}$ mbar, with the substrate holder rotating continuously to enhance film uniformity.

Electrical resistance measurements as a function of temperature (*R–T*) were performed using a specially designed resistance *vs.* temperature setup and a Keithley B2901B Source Measure Unit (SMU). The resistance was determined through the two-point probe technique, with the SMU recording resistance values across a range of temperatures. To explore crystallization effects, films in their as-deposited state were subjected to annealing at 100 °C, 200 °C, and 300 °C in a nitrogen environment. The as-deposited and annealed films are analyzed by scanning electron microscope (SEM) with a 2 kV source. The composition of various elements in the film is confirmed by the energy dispersive X-ray spectroscopy (EDS) technique by the same instrument. The device analysis was conducted on a sandwich-type device, fabricated by the thermal evaporation method, with aluminum serving as both the top and bottom electrodes. The surface morphology of the as-deposited samples and the cross-sectional thickness of each layer of the device were examined using a Zeiss Sigma 300 scanning electron microscope (SEM). The crystalline and amorphous characteristics of both the as-deposited and annealed samples were analyzed with a PANalytical X'Pert3 X-ray diffractometer, using a Cu-Kα source ($\lambda = 0.154$ nm).

The Keithley 2450 source measuring unit (SMU) was utilized to analyze the photo response by measuring the variation in the photo and dark current over a voltage range of −5 V to +5 V. A 9 W white LED bulb served as the illumination source, and photocurrent readings were recorded under both light and dark conditions by switching the light on and off. To define the effective surface area for measurement, the edges of the thin film were scratched to form a square with a side length of 0.5 cm (resulting in an area of 0.25 cm^2). The silver paste was applied to opposite sides of the film to establish conductive contacts for measurement.

III. Results and discussion

a. Temperature dependent resistance study

The resistance *versus* temperature (*R–T*) measurements were conducted on the samples in their as-deposited state to

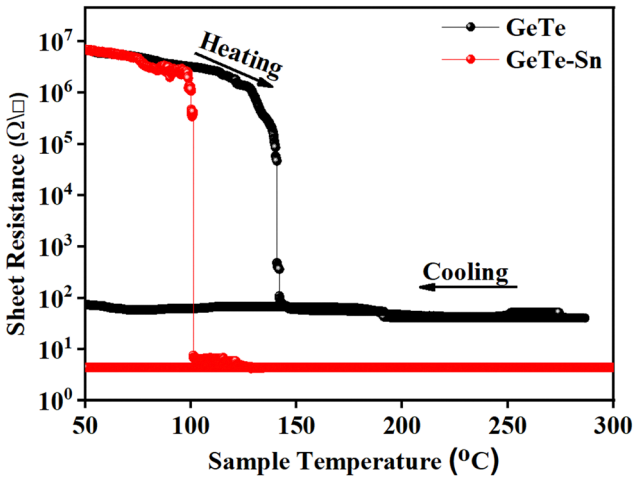

Fig. 1 Sheet resistance as function of temperature for GeTe and GeSnTe.

determine the transition characteristics from amorphous to crystalline phases. These resistance measurements were performed from room temperature up to 350 °C, with a heating rate of about 2.5 °C min^{-1}, as illustrated in Fig. 1. Resistance was also measured while cooling the sample (Fig. 1). The entire measurement process was conducted in a nitrogen atmosphere to prevent oxidation at high temperatures.

The resistance shows a continuous decrease with temperature until the crystallization temperature (T_c), then an abrupt drop, which indicates that an amorphous-to-crystalline transition has occurred. The T_c of GeTe is measured to be ~150 °C, and for GeSnTe is ~100 °C, showing a 50 °C reduction in the transition temperature. This shows that the substitution of Sn for Ge in GeTe will lead to easy crystallization. The resistance of the amorphous phase does not decrease at the initial state, which confirms that the hopping mechanism does not happen for both compositions.[24]

Though it is reported that the thermal stability of the amorphous state is decreased by the introduction of Sn,[25–28] our experiments suggest that the initial resistance of both alloys is almost the same. Amorphous phase stability in phase change materials (PCMs) is crucial for data preservation, especially at high temperatures when the data may be lost as the amorphous phase crystallises.[29] Amorphous chalcogenide PCM materials spontaneously and thermally crystallize, affecting reliability,[30] that may impact data stability. Standard PCM cells can store data for over 100 000 hours at 85 °C; however, higher temperatures limit this. As thought, retention lifespan may not follow the Arrhenius law according to temperature. At lower operating temperatures, non-Arrhenius nucleation hinders long-term data retention forecasts.[29] While cooling the samples, the resistance shows a small increase with decreasing temperature, which indicates that the crystallized samples are also semiconducting in nature.[31]

At the same time, Sn substitution decreases the resistance of the crystallized phase, which enhances the electrical resistivity contrast and therefore GeSnTe shows a higher contrast of 6 orders of magnitude. This shows a significant improvement for multi bit data storage by controlling the applied pulses for multiple memory applications. The slope of the R–T graph is used to compare the speed of phase transition. It is given by $\left(\frac{\Delta R}{\Delta T}\right)$ during the switching process. This slope -0.22×10^{-2} for GeTe and -1.442×10^{-2} Ω □$^{-1}$ °C^{-1} for GeSnTe. This indicates that the Sn-doped GeTe sample exhibits a steeper slope than the parent GeTe, resulting in a faster crystallization process for GeSnTe. This signifies that the process control is possible for crystallization speed. Although T_c decreases for the Sn substitution, the electrical resistivity contrast is enhanced. Notably, the fast crystallization speed likely transitions into a stable cubic phase (Fig. 2). This offers benefits in terms of controlled modifications for various synaptic pulses in neuromorphic computing. For instance, using Sn as a dopant or substituent in GeTe allows for precise tuning to a lower T_c. However, too much Sn can lead to higher resistance contrast and reduced data retention, making it crucial to optimize the Ge/Sn ratio for reliable memory performance. This study demonstrates that the T_c and resistance contrast can be tuned by Sn substitution for neuromorphic applications by controlling the spiking of variable voltages as needed, and may be beneficial for adjusting the power requirements of neuromorphic or PCM applications.

b. X-ray diffraction studies

Fig. 2 shows the XRD pattern of the as-deposited and annealed GeTe and GeSnTe films. The XRD pattern shows the phase transformation with temperature, resulting from atomic rearrangements. The increase in annealing temperature gives a crystalline pattern, which demonstrates that crystallization occurs above a certain critical temperature. This can match the T_c observed by R–T measurement. The patterns of the samples annealed above T_c represent the crystalline phase of the films.[32] Fig. 3a shows a black colored pattern without distinct peaks, confirming the amorphous nature of the as-deposited GeTe samples. Upon annealing at 300 °C, XRD peaks verify the crystalline nature of the GeTe sample. The crystalline peaks exactly match with standard ICSD pattern (ICDD-00-047-1079). The GeTe was found to crystallize in a rhombohedral structure with the $R3mH$ space group.

The as-deposited GeSnTe sample shows the presence of crystalline features, confirming the easy crystallization possibility when Sn substitutes for Ge. Annealing at 300 °C, the crystalline phase evolved with a cubic structure (ICDD-01-071-4742), which shows GeSnTe undergoes a phase transition to a cubic structure when the Sn amount is about 50%. At higher level of substitution such as 50%, Sn may also occupy some interstitial sites rather than substitutional ones, causing significant local distortions that further fragment crystallites. The broadening of crystalline peaks for GeSnTe is because of two reasons, one is the reduction of the crystallite size with addition of Sn and second, Sn substitution causes uneven lattice stretching, leading to variations in interplanar spacing (d-spacing). This microstrain may be another reason for the broadening of XRD peaks.

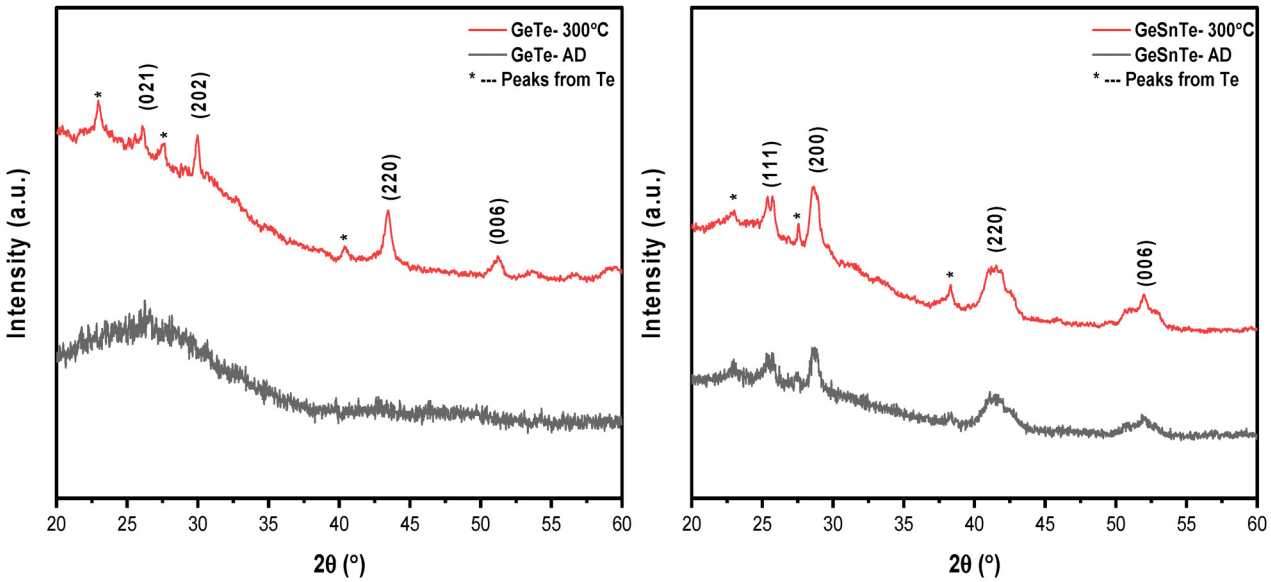

Fig. 2 XRD pattern of (a) GeTe and (b) GeSnTe thin films.

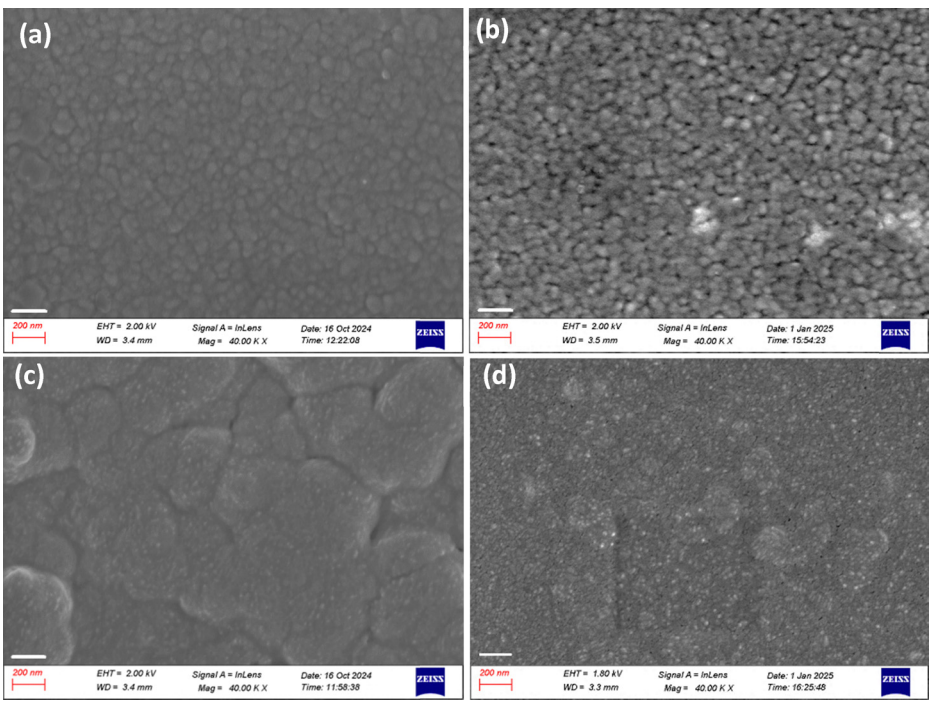

Fig. 3 SEM images of GeTe, (a) as-deposited (b) annealed at 300 °C, GeSnTe (c) as deposited, and (d) annealed at 300 °C.

At high temperature, pure GeTe exhibits a rhombohedral structure ($R3m$) due to Peierls instability-induced distortion. Introducing Sn as a dopant reduces this distortion, steering the structure toward a cubic (rock-salt) form similar to SnTe. This is similar to the rhombohedral structure of GeTe being modified to a simpler cubic structure in the presence of Sn. This shift is due to Sn's inclination for cubic symmetry, as observed in the NaCl-type structure of SnTe. Sn^{2+} has an ionic radius of 1.40 Å, which is larger than Ge^{2+}, which has an ionic radius of 0.87 Å. Replacing Ge with Sn leads to local lattice distortions because of this size difference. This strain disrupts the lattice's long-range order, breaking crystallites into smaller domains (crystallite size reduction) or causing uneven lattice spacing (microstrain). Amorphous to cubic structure transformation is more favorable than amorphous to rhombohedral transformation; the system is easily transformable to a cubic structure corresponding to a lower T_c.

Additionally, Sn substitution did not add any phase precipitation, especially Ge phases, as shown by the absence of Ge peaks in XRD. Tellurium peaks were observed (ICDD-01-086-2268), indicatingthat Te segregates during the sample preparation process. The segregation of Te may be because of the lower activation energy for diffusion compared to Ge and Sn, which results in more mobility of Te during the phase change process, causing segregation of Te in crystallization, and because when Sn is bonded with Ge, some Ge–Te bonds are formed, leaving some Te segregation.

c. SEM analysis

Fig. 3 shows the surface morphology of the as-deposited and annealed samples at various magnifications. Both the as-deposited samples (Fig. 3a and c) exhibit uniform morphology without any signs of cracks. SEM of GeTe shows surface characteristics like uniform distribution of small particles, boundaries, and the distribution of amorphous phases. The surface features of GeSnTe show well rounded features different from the GeTe samples. Annealed samples at 300 °C (Fig. 3b and d) show the more distinct boundaries, which indicate the crystallization induced changes.

The incorporation of Sn can alter surface uniformity and grain arrangement. Sn doping leads to grain refinement by decreasing size and encouraging denser packing, resulting in uniform grain formations in GeSnTe. These alterations have the potential to influence the material's electrical and optical properties, both of which are exceptionally important for the performance of PCM and neuro-inspired computing devices.

The reduced crystallite size, as shown from X-ray diffraction study and confirmed by surface morphological analysis, reveals that the Sn doping can bring the high endurance of devices. Smaller grains in the devices result in more grain boundaries, which hinder atom mobility and reduce unwanted diffusion and elemental segregation over repeated cycling. The phase change process will be stabilised, and the device life will be extended by this homogeneous and fine-grained structure. A higher grain boundary density traps defects and restricts their spread during repeated switching cycles by acting as a barrier to atom migration and phase segregation.

d. Optical studies

For optical phase change applications, the difference in reflectance between the crystalline and amorphous phases of phase change memory materials is utilised. Transmission spectra of GeTe and GeSnTe thin films are shown in Fig. 4.

Reflectivity is higher in the crystalline phase and lower in the amorphous phase. The increase in reflection is linked to the observed decrease in transmission in crystallised films. The transmittance spectra show a significant difference between the crystallised samples and the amorphous samples (Fig. 4a and c). In the amorphous state, low transmittance is observed at shorter wavelengths, indicating a larger bandgap, which is consistent with amorphous materials' lower conductivity.[24] The transmission was studied with various annealing temperatures, which reveals that the transmittance edge is different before and after the phase change. This is observed for both GeTe and GeSnTe. This is because the optical band gap is reduced when amorphous changes to crystalline structure.

The optical band gap was calculated using the Tauc model and the formula,[33]

$$(\alpha h\nu)^{1/2} = B^{1/2}\,(h\nu - E_{\mathrm{opt}}) \quad (1)$$

E_{opt} stands for the optical bandgap, ν for frequency, h for Planck's constant, α for the absorption coefficient, and $B^{1/2}$ for the Tauc parameter. The Tauc plots for both samples are plotted in Fig. 4b and d. Table 1 presents the optical bandgap values obtained from the Tauc plot, illustrating how the bandgap varies with annealing temperature.

When amorphous GeTe changes to crystalline GeTe during phase transition, a new rhombohedral structure is formed with some vacancies. A reported optical bandgap of GeTe is ~0.48 eV.[34] So, this transition is accompanied by a vacancy formation in GeTe lattice resulting a band gap shown in Fig. 4. In the case of GeSnTe, when the Sn atom replaces Ge, the system forms a cubic lattice which is symmetrically preferred than rhombohedral latiice. There is a possibility that the vacancies are already removed in the phase formation. And a corresponding band gap is observed. This tends to be a higher value with respect to the GeTe. When GeTe is doped with Sn, its optical band gap decreases due to a number of interrelated factors that cause the change in electronic structure of the material. Atomic level disorder and lattice distortion brought about by Sn substitution disturb bonding environments and electronic states. Sn–Te bond formation increases ionicity and defect states by altering the local chemical environment. Band edges move closer together as a result of these modifications, which reduce the energy differential between the valence and conduction bands.[35,36] The band gap is further reduced by Sn doping, which also lessens Peierls distortion and tetrahedral motifs in the amorphous phase. The density of electronic states close to band edges is impacted by the narrowing of the band gap, which is associated with elevated levels of disorder and defects.[37] By altering optical and electrical switching characteristics that are essential to device performance, these changes have a substantial impact on PCM applications. By adjusting optical contrast and possibly boosting thermal stability, Sn doping improves the performance of PCM devices.

e. *I–V* switching studies

The proper way to study switching and memory effects in amorphous chalcogenide semiconductors is through the electro-thermal mechanism. Joule heating produces the thermal effects, whereas the applied field that transforms the materials from an amorphous to a crystalline state produces the electronic effects. This model heavily considers the possibility that defect states retain charge carriers.[38]

Fig. 5 is the electrical switching behavior of the PCM devices based on GeTe and GeSnTe. The sandwich type device with Al (40 nm)/PCM (260 nm)/Al (40 nm) was fabricated on a glass substrate is shown in Fig. 5a and its schematic is shown in Fig. 5b. The electrical switching study (Fig. 5c and d), is reveals

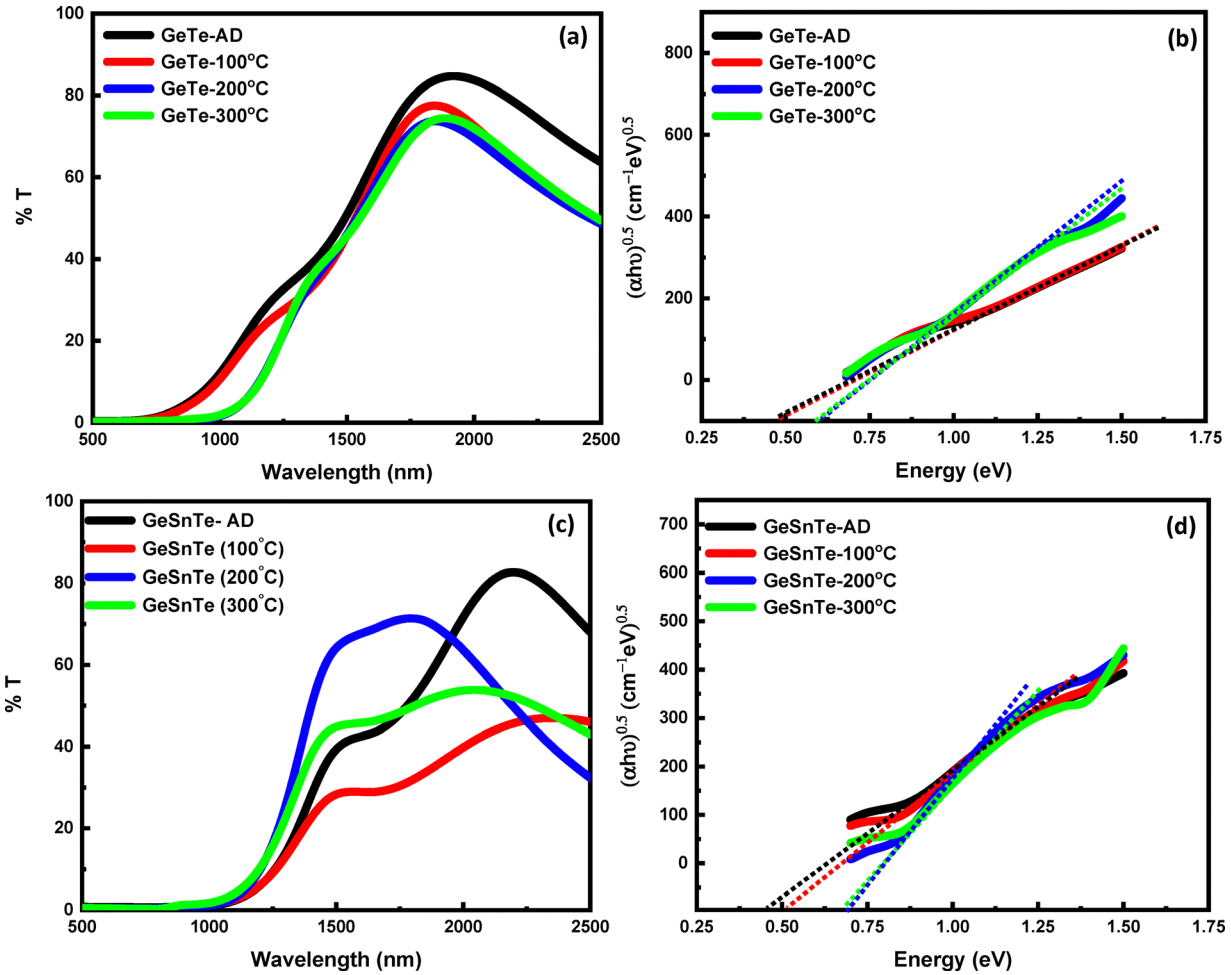

Fig. 4 Shows UV-Vis-NIR transmission spectra of GeTe and GeSnTe at various annealing temperatures.

Table 1 Calculated optical bandgap for each sample using Tauc plot

	Optical band gap (eV)	
	GeTe	GeSnTe
AD	0.466	0.443
100 °C	0.48	0.504
200 °C	0.604	0.697
300 °C	0.591	0.671

that the current is not increasing with voltage (non-Ohmic behavior) until a threshold voltage (V_{th}) which can be termed as amorphous (OFF) state. After V_{th}, an abrupt increase in current which is shows the phase transition of the device. The Ohmic behavior of current and voltage after V_{th} is the crystalline ON state. V_{th} observed for the GeTe is 4.5 V and GeSnTe is 2.46 V. This decrease in V_{th}, by substituting Sn to Ge which is because of low T_c observed from R–T measurement. This can be analyzed as, the Sn incorporation decreases the network connectivity, making the structural rearrangement easier, which is to cubic structure. The changes in the resistance slope by orders of magnitude is depending on whether the material in the active region of the device is crystalline or amorphous. To reach the switching regions, the bias is raised above the threshold voltage so that enough current will pass through the cell, by Joule heating of the active area, which gets heated up and results in amorphous to crystalline phase change.[39] The graph shows the amorphous region with the increase of the bias causes a rapid increase in current due to an abrupt drop in electrical resistivity of the phase change material that causes the crystallization. The number of charge carriers increases drastically after the threshold voltage, which causes a decrease in resistance of the PCM.

f. Photo-response study

The photoresponse study was carried out for the as deposited and annealed films. This study reveals the effects of annealing at different temperatures on the photodetection performance of the material. Schematic for I–V measurement setup of the GeSnTe films, as illustrated in Fig. 6.

The photocurrent (I_{ph}) is defined as the difference in the current values between external light illumination (I_L) and without light illumination (I_D), *i.e.*,

$$I_{ph} = I_L - I_D \quad (2)$$

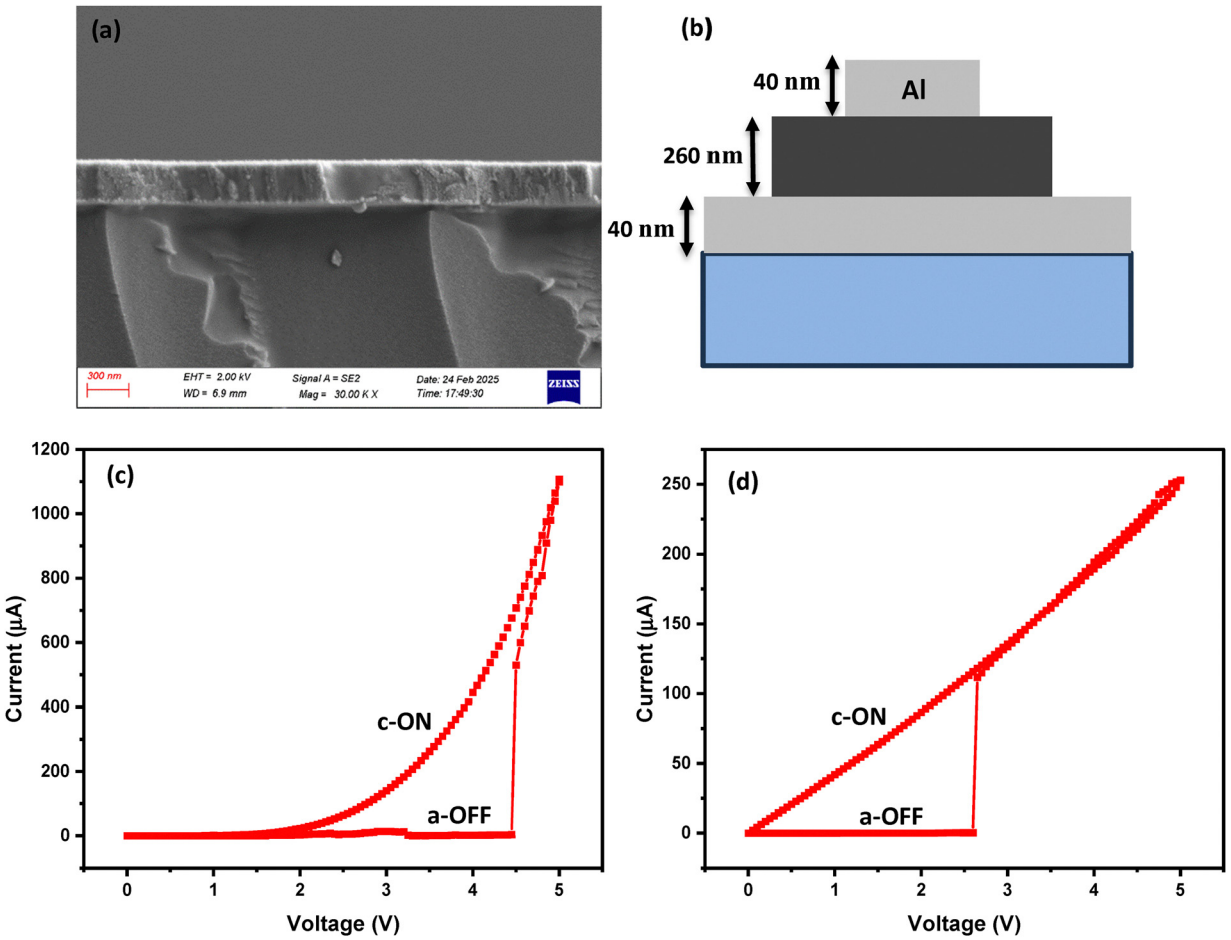

Fig. 5 (a) Cross sectional SEM, (b) schematic of device and *I*–*V* study of (c) GeTe and (d) GeSnTe based devices which shows threshold voltages of 4.5 V and 2.63 V respectively.

The photocurrent (I_{ph}) values for all film samples are presented in Table 2.

The photosensitivity of the thin films is calculated using the formula given in eqn (3). An increase in annealing temperature enhances the photodetector's performance by improving crystallinity, leading to higher photoresponsivity and detectivity.[40,41]

The performance of a photodetector under both low- and high-light conditions is primarily governed by the generation of electron–hole pairs, which is proportional to the incident light power density. Upon illumination, these electron–hole pairs contribute to an increase in photocurrent. Additionally, key performance parameters such as photoresponsivity (R) and detectivity (D^*) are essential for evaluating the efficiency of photodetectors.[41] These parameters are calculated using specific mathematical expressions and are also summarized in Table 2.

$$\text{Photo sensitivity} = \frac{I_{ph}}{I_D} \times 100\% \quad (3)$$

$$\text{Responsivity}\,(R) = \frac{I_L}{A \times P_{in}} \quad (4)$$

$$\text{Detectivity}\,(D*) = R\sqrt{\frac{A}{2eI_D}} \quad (5)$$

In this context, A refers to the active surface area of the photodetector, which is 0.25 cm^2. P_{in} denotes the incident light power density, measured as 20 mW cm^{-2}. Additionally, e represents the elementary charge of an electron, h corresponds to Planck's constant, λ signifies the wavelength of the incident light, and c denotes the speed of photons.

$$\text{Noise equivalent power (NEP)} = \frac{\sqrt{2eI_D}}{R} \quad (6)$$

The noise-equivalent power (NEP) represents the smallest optical power that produces a signal equal to the detector's inherent noise level; thus, a lower NEP value signifies higher sensitivity and an improved ability to detect weak optical signals.

The NEP values presented in Table 2 highlight the high sensitivity of both GeTe and GeSnTe thin-film photodetectors. A noticeable decrease in NEP with annealing temperature is observed for GeTe, with the lowest value (6.02×10^{-10} W $Hz^{-1/2}$) at 300 °C, indicating improved crystallinity and reduced noise. For GeSnTe, the 200 °C annealed sample exhibits the optimal

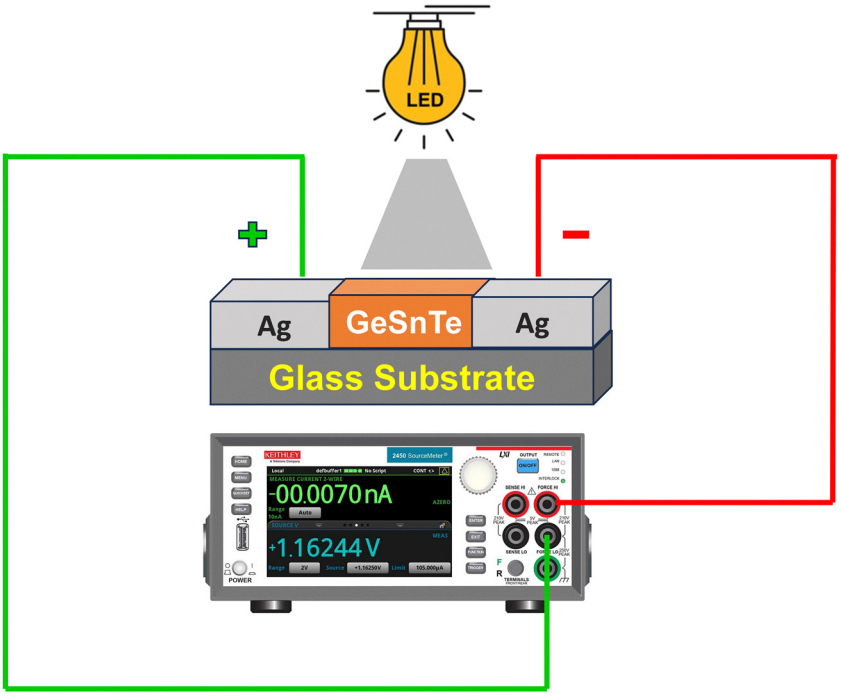

Fig. 6 Schematic for *I*–*V* photo response measurement setup.

Table 2 The figure for the merits of all the thin films annealed in GeTe and GeSnTe

Sample	I_L (A)	I_D (A)	I_{ph} (A)	Photo sensitivity (%)	Responsivity (R) (A W^{-1})	Detectivity (D^*) (Jones)	NEP (WHz$^{-1/2}$)
GeTe-AD	6.34×10^{-8}	5.14×10^{-8}	1.19×10^{-8}	23.29	1.26×10^{-5}	4.94×10^{7}	1.01×10^{-8}
GeTe-100 °C	7.33×10^{-8}	3.48×10^{-8}	3.85×10^{-8}	110.64	1.46×10^{-5}	6.94×10^{7}	7.19×10^{-9}
GeTe-200 °C	5.86×10^{-4}	5.77×10^{-4}	9.07×10^{-6}	1.65	1.17×10^{-1}	4.31×10^{9}	1.16×10^{-10}
GeTe-300 °C	9.54×10^{-6}	4.12×10^{-6}	5.42×10^{-6}	131.57	1.91×10^{-3}	8.31×10^{8}	6.02×10^{-10}
GeSnTe-AD	4.54×10^{-6}	3.38×10^{-6}	1.15×10^{-6}	34.11	9.08×10^{-4}	4.36×10^{8}	1.46×10^{-9}
GeSnTe-100 °C	1×10^{-1}	9.60×10^{-2}	3.96×10^{-3}	4.12	19.99	5.7×10^{10}	8.77×10^{-12}
GeSnTe-200 °C	6.81×10^{-2}	4.84×10^{-2}	1.97×10^{-2}	40.63	13.63	5.47×10^{10}	9.13×10^{-12}
GeSnTe-300 °C	6.21×10^{-3}	5.06×10^{-3}	1.15×10^{-3}	22.83	1.24	1.54×10^{10}	3.24×10^{-11}

balance of low NEP (9.13×10^{-10} W Hz$^{-1/2}$), high responsivity (13.63 A W^{-1}), and detectivity (5.47×10^{10} Jones), confirming that Sn incorporation enhances photodetection sensitivity and signal-to-noise performance.

Fig. 7 presents the *I*–*V* characteristics of GeTe film photodetectors annealed at different temperatures, measured under both dark and illuminated conditions. The illumination is provided by a 9 W white LED bulb, delivering a power density of 20 mW cm^{-2} at room temperature. The results clearly show an increase in current for all samples (as deposited and annealed), when exposed to LED light illumination. This is attributed to the enhanced generation of photocarriers within the GeTe and GeSnTe films, confirming the conventional photoconductive effect.

Fig. 7(a)–(f) illustrate the photoresponse behavior of the GeTe film photodetector under dark and illuminated conditions. The plots exhibit distinct and symmetric *I*–*V* curves for each thin film, consistently showing a higher photocurrent compared to the dark current. This increase in photocurrent results from light-material interactions and charge carrier separation.[42] When photons with energy exceeding the material's band gap are absorbed by the GeTe film, electron–hole pairs are generated and separated under the applied bias voltage. These charge carriers move in opposite directions, leading to the generation of a photocurrent.[40] The GeTe thin film samples exhibit a clear dependence of photoresponse on annealing temperature. The *I*–*V* plot of as-deposited sample in Fig. 7(a) shows minimal photoresponse, with nearly overlapping *I*–*V* curves under dark and illuminated conditions. However, as the annealing temperature increases to 100 °C, 200 °C, and especially 300 °C as displayed in Fig. 7(b)–(d), a significant enhancement in photocurrent is observed, particularly at higher voltages. This is further supported by the dark and light current plots shown in Fig. 7(e) and (f), where the 300 °C annealed film demonstrates a pronounced increase in current under illumination, indicating improved photoconductivity. These results suggest that thermal annealing facilitates structural or phase transformations in GeTe, thereby enhancing

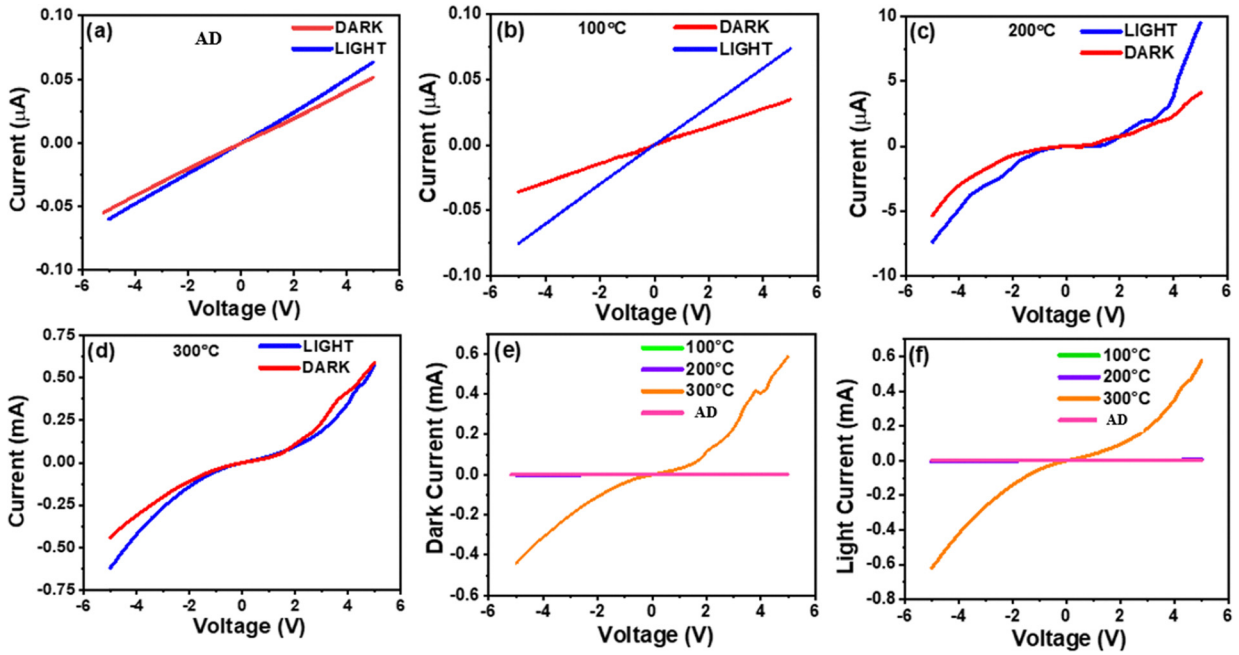

Fig. 7 *I–V* characteristic plot of GeTe thin films (a) as deposited, annealed at (b) 100, (c) 200, and (d) 300 °C. Current response is also shown in both (e) dark and (f) light conditions.

carrier mobility and light absorption, crucial for optoelectronic performance.

The *I–V* characteristics shown in Fig. 8 reveal that GeSnTe thin films demonstrate a significant photoresponse enhancement with increasing annealing temperature. Under light, more photocurrent is produced in all cases and at 100 °C (Fig. 8b) and 200 °C (Fig. 8c) annealed samples show a clear contrast wrt 300 °C annealed sample (Fig. 8d) with very high current in the order of 10 s of mA. As evident in the Fig. 8e and f, light current is relatively higher for all samples wrt the dark current. While the as-deposited and 100 °C, 300 °C-annealed samples as displayed in Fig. 8(a), (b) and (d) exhibit negligible

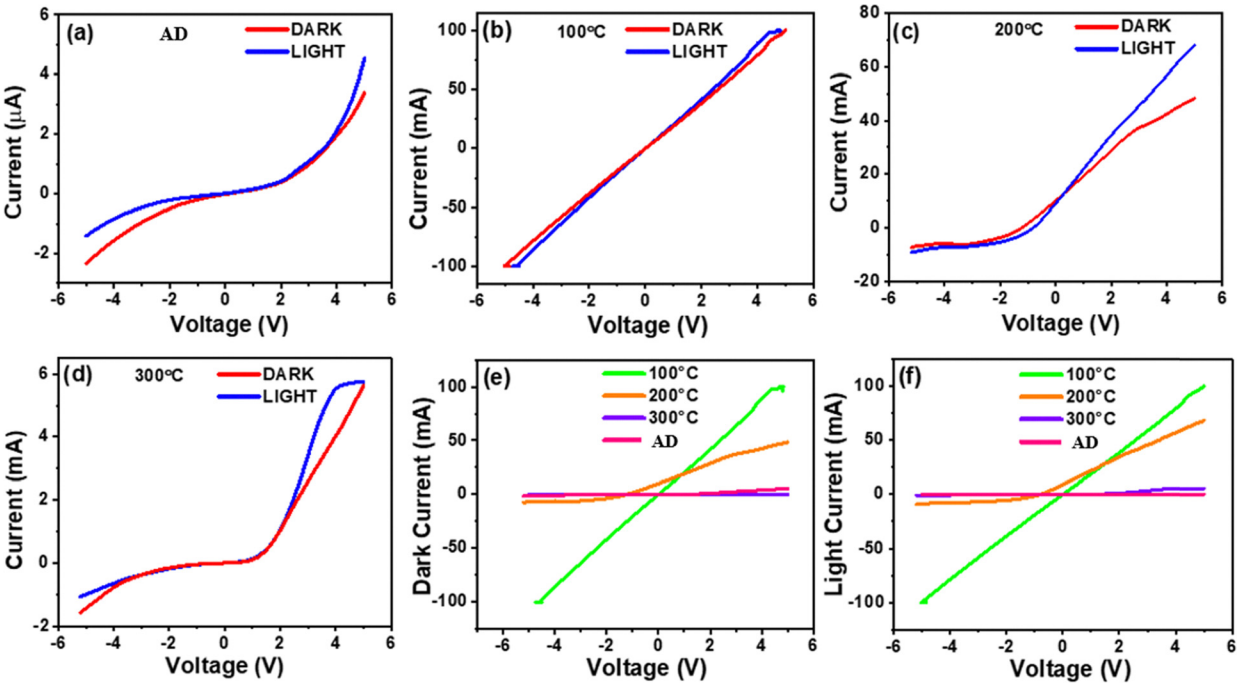

Fig. 8 *I–V* characteristic plot of GeSnTe thin films (a) as deposited, (b) annealed at 100, (c) 200, and (d) 300 °C. Current response in both (e) dark and (f) light conditions is also shown.

differences between dark and light currents, sample annealed at 200 °C shown in Fig. 8(c) show a marked increase in photocurrent, particularly at higher voltages. This is further validated by the comparative dark and light current plots demonstrated in Fig. 8(e) and (f), where the 100 °C-annealed film shows the highest photocurrent, indicating substantial photoactivation. These findings suggest that Sn incorporation combined with thermal annealing improves the crystalline quality and carrier transport, thereby enhancing the optoelectronic response of GeSnTe films for potential applications in light-sensitive devices.

All samples exhibit significant photosensitivity; however, the GeTe sample annealed at 200 °C demonstrates the best photodetection performance within its set. Similarly, the GeSnTe sample annealed at 100 °C show superior values for key photodetection parameters compared to other samples in the set. The Ag metallic contacts efficiently extract most of the photogenerated carriers to contribute to the photocurrent, while additional mechanisms, such as hole trapping due to defect states, may also play a crucial role in photocurrent generation.[43] The photodetection properties, including responsivity and detectivity, are influenced by both the crystallization and carrier mobility of the materials. Although the variations in photodetection parameters with respect to annealing temperature do not follow a strictly defined trend, the results highlight the potential for further research and optimization of both the sample preparation process and measurement techniques. This study suggests that GeTe and GeSnTe-based thin films hold significant promise as effective alternatives for photodetector applications.

The photoresponse parameters presented in Table 2 highlight distinct trends in GeTe and GeSnTe thin films with respect to annealing temperature. For GeTe samples, annealing at 300 °C yields the highest photosensitivity (131.57%), responsivity (1.91×10^{-4} A W^{-1}), and detectivity (8.31×10^{8} Jones), indicating enhanced optoelectronic performance due to improved crystallinity and carrier dynamics. In contrast, GeSnTe samples exhibit significantly higher absolute photocurrent levels, with the GeSnTe-200 °C film showing a peak in responsivity (13.63 A W^{-1}) and detectivity (5.47×10^{10} Jones) far exceeding those of GeTe, despite a relatively lower photosensitivity (40.63%). These results suggest that Sn incorporation significantly boosts photodetector metrics, particularly in terms of signal strength and noise performance.

IV. Conclusion

Phase change material GeTe is designed by substituting Ge with Sn to reduce the system's overall cost and finding the suitability for memory applications. The resistance *vs.* temperature measurements show the transition temperature of GeTe is ~150 °C and $Ge_{0.5}Sn_{0.5}Te$ is ~100 °C with a contrast of 5 and 6 orders of magnitude respectively. The experimental results indicate that the incorporation of Sn in GeTe-based PCM materials may help to tune the performance characteristics, including controlled crystallization to cubic phase, band structure modification, and the stabilization of targeted phases. Sn inclusion stabilizes the cubic phase at lower temperatures and influences the crystallization pathway. Due to the lower transition temperature and band gap in Sn-doped GeTe samples, the phase transition occurs at reduced power levels, indicating that the power consumption required for phase transition is less for GeSnTe compared to GeTe. This also gives an advantage of controlling the set-reset requirements for the neuromorphic applications. This study also show that this novel compound design can be used for electrical resistance contrast tuning, which can be of formidable importance for neuromorphic computing and multi-bit memory applications. Enhancement in optical properties like transmission edge and reduction in optical band gap for the Sn incorporation and its reasons has been analyzed. The photoresponse study conducted for both GeTe and GeSnTe thin films show good photoresponsivity and other critical parameters like responsivity and detectivity. These parameters of the prepared films indicate the effects of annealing the samples at different temperatures on the photodetection performance of the material. The present study covers the path for exploring the potential of these materials for becoming an effective photodetection device in the future, since Sn incorporation enhances the photo detectivity. Nonetheless, careful optimization of the Sn content is crucial to find potential uses in both PCRAM and neuromorphic applications.

Author contributions

MNK was responsible for preparing samples, conducting characterizations, performing analyses and drafting the original manuscript. RSS contributed to sample preparations and editing the manuscript. PCK performed photoresponse characterizations, result analysis and manuscript modification. RN planned, supervised photoresponse experiment and reviewed the manuscript. VEM supervised and reviewed the work, provided critical feedback, and finalized the manuscript.

Conflicts of interest

The authors declare no competing financial interests.

Data availability

The data and figures generated and/or analyzed during the current study are available on request. The figures are open to the public under the condition that any use of the data is credited appropriately according to the citation guidelines provided.

Acknowledgements

The authors express their sincere gratitude for the financial assistance provided by the Science and Engineering Research Board (SERB File no: SRG/2023/001476), Faculty Research Grant (NITC/(R&C)/2023-2024/FRG/PhaseIII/(71)) and University Grants Commission, Ministry of Education India (Junior

Research Fellowship) for providing the essential resources and funding that facilitated the successful completion of this research. The authors would also like to acknowledge the FIST-funded (FIST No. SR/FST/ET-I/2021/840) SEM Centre at the Department of Materials Science and Engineering at NITC for the SEM characterization. Furthermore, we acknowledge the *R–T* measurement facility at Indian Institute of Science, Central XRD facility and Raman facility at NITC for conducting characterisations.

References

1 S. Raoux, G. W. Burr, M. J. Breitwisch, C. T. Rettner, Y. C. Chen, R. M. Shelby, M. Salinga, D. Krebs, S. H. Chen, H. L. Lung and C. H. Lam, Phase-Change Random Access Memory: A Scalable Technology, *IBM J. Res. Dev.*, 2008, **52**(4–5), 465–479, DOI: 10.1147/rd.524.0465.

2 P. Guo, A. M. Sarangan and I. Agha, A Review of Germanium-Antimony-Telluride Phase Change Materials for Non-Volatile Memories and Optical Modulators, *Appl. Sci.*, 2019, **9**(3), 530, DOI: 10.3390/app9030530.

3 S. R. Nandakumar, M. Le Gallo, I. Boybat, B. Rajendran, A. Sebastian and E. Eleftheriou, A Phase-Change Memory Model for Neuromorphic Computing, *J. Appl. Phys.*, 2018, **124**(15), 152135, DOI: 10.1063/1.5042408.

4 Y. Chen, L. Sun, Y. Zhou, G. M. Zewdie, V. L. Deringer, R. Mazzarello and W. Zhang, Chemical Understanding of Resistance Drift Suppression in Ge-Sn-Te Phase-Change Memory Materials, *J. Mater. Chem. C Mater.*, 2019, **8**(1), 71–77, DOI: 10.1039/c9tc04810c.

5 H. S. P. Wong; S. Raoux; S. Kim; J. Liang; J. P. Reifenberg; B. Rajendran; M. Asheghi and K. E. Goodson, Phase Change Memory, *Proceedings of the IEEE*, Institute of Electrical and Electronics Engineers Inc., 2010, vol. 98, pp 2201–2227, DOI: 10.1109/JPROC.2010.2070050.

6 J. Pady, J. Costa, C. Ramsdale, F. Alkhalil, A. Nevill, M. F. Craciun and C. D. Wright, Flexible Electronics Applications of Ge-Rich and Se-Substituted Phase-Change Materials in Nonvolatile Memories, *Phys. Status Solidi – Rapid Res. Lett.*, 2024, **18**(10), 2300425, DOI: 10.1002/pssr.202300425.

7 S. Wintersteller, O. Yarema, D. Kumaar, F. M. Schenk, O. V. Safonova, P. M. Abdala, V. Wood and M. Yarema, Unravelling the Amorphous Structure and Crystallization Mechanism of GeTe Phase Change Memory Materials, *Nat. Commun.*, 2024, **15**, 1011, DOI: 10.1038/s41467-024-45327-7.

8 M. Le Gallo and A. Sebastian, An Overview of Phase-Change Memory Device Physics, *J. Phys. D*, 2020, **53**(21), 213002, DOI: 10.1088/1361-6463/ab7794.

9 N. Bala, B. Khan, K. Singh, P. Singh, A. P. Singh and A. Thakur, Recent Advances in Doped $Ge_2Sb_2Te_5$ Thin Film Based Phase Change Memories, *Mater. Adv. R. Soc. Chem.*, 2022, **4**, 747–768, DOI: 10.1039/d2ma01047j.

10 P. Gupta, P. Lohia and D. K. Dwivedi, Phase Change Memory: Operation, Current Challenges and Future Prospects, *Int. J. Eng., Sci. Technol.*, 2021, **13**(1), 93–97, DOI: 10.4314/ijest.v13i1.14s.

11 Y. Zeng, G. Ma, H. Li, X. Cheng and X. Miao, Significant Power Consumption Reduction and Speed Boosting in Phase Change Memory with Nanocurrent Channels, *Nano Lett.*, 2024, **24**(40), 12658–12665, DOI: 10.1021/acs.nanolett.4c03900.

12 K. Ren, M. Zhu, W. Song, S. Lv, M. Xia, Y. Wang, Y. Lu, Z. Ji and Z. Song, Electrical Switching Properties and Structural Characteristics of GeSe-GeTe Films, *Nanoscale*, 2019, **11**(4), 1595–1603, DOI: 10.1039/c8nr07832g.

13 R. O. Jones, Phase Change Memory Materials: Why Are Alloys of Ge, Sb, and Te the Materials of Choice?, *Solid State Sci.*, 2024, 152, DOI: 10.1016/j.solidstatesciences.2024.107524.

14 Y. Zheng, W. Song, Z. Song, Y. Zhang, T. Xin, C. Liu, Y. Xue, S. Song, B. Liu, X. Lin, V. G. Kuznetsov, I. I. Tupitsyn, A. V. Kolobov and Y. Cheng, A Complicated Route from Disorder to Order in Antimony–Tellurium Binary Phase Change Materials, *Adv. Sci.*, 2024, **11**(9), 2301021, DOI: 10.1002/advs.202301021.

15 B. G. Sangeetha, C. M. Joseph and K. Suresh, Preparation and Characterization of $Ge_1Sb_2Te_4$ Thin Films for Phase Change Memory Applications, *Microelectron. Eng.*, 2014, **127**, 77–80, DOI: 10.1016/j.mee.2014.04.032.

16 Q. Wang, B. Liu, Y. Xia, Y. Zheng, R. Huo, Q. Zhang, S. Song, Y. Cheng, Z. Song and S. Feng, Cr-Doped $Ge_2Sb_2Te_5$ for Ultra-Long Data Retention Phase Change Memory, *Appl. Phys. Lett.*, 2015, **107**(22), 222101, DOI: 10.1063/1.4936847.

17 J. H. Han, K. S. Jeong, M. Ahn, D. H. Lim, W. J. Yang, S. Jong Park and M. H. Cho, Modulation of Phase Change Characteristics in Ag-Incorporated $Ge_2Sb_2Te_5$ Owing to Changes in Structural Distortion and Bond Strength, *J. Mater. Chem. C Mater.*, 2017, 5(16), 3973–3982, DOI: 10.1039/c6tc05412a.

18 G. Wang, Q. Nie, X. Shen, R. P. Wang, L. Wu, J. Fu, T. Xu and S. Dai, Phase Change Behaviors of Zn-Doped $Ge_2Sb_2Te_5$ Films, *Appl. Phys. Lett.*, 2012, **101**(5), 051906, DOI: 10.1063/1.4742144.

19 T. J. Park, S. Y. Choi and M. J. Kang, Phase Transition Characteristics of Bi/Sn Doped $Ge_2Sb_2Te_5$ thin Film for PRAM Application, *Thin Solid Films*, 2007, **515**(12), 5049–5053, DOI: 10.1016/j.tsf.2006.10.045.

20 W. D. Song, L. P. Shi, X. S. Miao and T. C. Chong, Phase Change Behaviors of Sn-Doped Ge-Sb-Te Material, *Appl. Phys. Lett.*, 2007, **90**(9), 091904, DOI: 10.1063/1.2475390.

21 W. Q. Li, F. R. Liu, Y. Z. Zhang, G. Han, W. N. Han, F. Liu and N. X. Sun, Crystallization Accompanied by Local Distortion Behavior of Sn-Doped Amorphous $Ge_2Sb_2Te_5$ Induced by a Picosecond Pulsed Laser, *J. Non-Cryst. Solids*, 2019, **516**, 99–105, DOI: 10.1016/j.jnoncrysol.2019.04.004.

22 N. Bai, F. R. Liu, X. X. Han, Z. Zhu, F. Liu, X. Lin and N. X. Sun, Effect of the Sn Dopant on the Crystallization of Amorphous $Ge_2Sb_2Te_5$ Films Induced by an Excimer Laser, *Opt. Laser Technol.*, 2015, **74**, 11–15, DOI: 10.1016/j.optlastec.2015.03.019.

23 J. Y. Raty, W. Zhang, J. Luckas, C. Chen, R. Mazzarello, C. Bichara and M. Wuttig, Aging Mechanisms in Amorphous Phase-Change Materials, *Nat. Commun.*, 2015, **6**, 7467, DOI: 10.1038/ncomms8467.

24 R. Kemparaju, S. Rohit, A. Prabhudesai, S. C. Prasanth, M. M. Kumar and K. Ramesh, Electrical Switching and Phase Change Properties of GeTe-Al_2Te_3 Chalcogenide Alloys, *Ceram. Int.*, 2025, **51**(19), 29046–29054, DOI: 10.1016/j.ceramint.2025.04.110.

25 R. Lan, S. L. Otoo, P. Yuan, P. Wang, Y. Yuan and X. Jiang, Thermoelectric Properties of Sn Doped GeTe Thin Films, *Appl. Surf. Sci.*, 2020, **507**, DOI: 10.1016/j.apsusc.2019.145025.

26 D. Sidharth, A. R. Muchtar, A. S. A. Nedunchezhian, M. Arivanandhan and R. Jayavel, Thermoelectric Performance of Ge1-XSnxTe ($0 \leq x \leq 0.2$) Prepared by Facile Method, *J. Solid State Chem.*, 2022, **310**, 122995, DOI: 10.1016/j.jssc.2022.122995.

27 A. M. Ahmed, Electrical Conductivity and Thermoelectric Power of $Ge_{40}Te_{60}$ and $Ge_{38}Sn_2Te_{60}$ Alloys, *Indian J. Pure Appl. Phys.*, 2005, **43**, 535–541.

28 R. Lan, S. L. Otoo, P. Yuan, P. Wang, Y. Yuan and X. Jiang, Thermoelectric Properties of Sn Doped GeTe Thin Films, *Appl. Surf. Sci.*, 2020, **507**, 145025, DOI: 10.1016/j.apsusc.2019.145025.

29 B. Gleixner; A. Pirovano; J. Sarkar; F. Ottogalli; E. Tortorelli and M. Tosi; R. Bez Data Retention Characterization Of Phase-Change Memory Arrays.

30 J. Pries, C. Stenz, S. Wei, M. Wuttig and P. Lucas, Structural Relaxation of Amorphous Phase Change Materials at Room Temperature, *J. Appl. Phys.*, 2024, **135**(13), 135101, DOI: 10.1063/5.0198312.

31 R. Shekhawat, H. Pamuluri, V. Erkkara Madhavan and K. Ramesh, Structural Transformation and Phase Change Properties of Se Substituted GeTe, *Sci. Rep.*, 2021, **11**, 7604, DOI: 10.1038/s41598-021-87206-x.

32 G. Carotenuto, M. Palomba, S. De Nicola, G. Ambrosone and U. Coscia, Structural and Photoconductivity Properties of Tellurium/PMMA Films, *Nanoscale Res. Lett.*, 2015, **10**(313), 1–8, DOI: 10.1186/s11671-015-1007-z.

33 S. Parvanov, V. Vassilev and K. Tomova, Optical Properties of New Chalcogenide Glasses from the $GeSe_2$–Sb_2Se_3–PbSe System, *Mater. Lett.*, 2008, **62**(12–13), 2021–2024, DOI: 10.1016/j.matlet.2007.11.029.

34 S. Palaz; H. Koc; A. M. Mamedov and E. Ozbay, Topological Insulators: Electronic Band Structure and Spectroscopy, *IOP Conference Series: Materials Science and Engineering*, Institute of Physics Publishing, 2017, vol. 175, DOI: 10.1088/1757-899X/175/1/012004.

35 J. Zhang, H. Yu, F. Wei, Y. Dong, Z. Shao and Y. Liu, Sn Tuned Microstructure and Phase-Change Characteristics of GeTe Nanowires, *AIP Adv.*, 2020, **10**(10), 105228, DOI: 10.1063/5.0027144.

36 I. Hamberg, C. G. Granqvist, K.-F. Berggren, B. E. Sernelius and L. Engstrom, Band-gap widening in heavily Sn-doped In_2O_3, *Phys. Rev. B: Condens. Matter Mater. Phys.*, 1984, **30**, 3240, DOI: 10.1103/PhysRevB.30.3240.

37 R. Lan, S. L. Otoo, P. Yuan, P. Wang, Y. Yuan and X. Jiang, Thermoelectric Properties of Sn Doped GeTe Thin Films, *Appl. Surf. Sci.*, 2020, **507**, 145025, DOI: 10.1016/J.APSUSC.2019.145025.

38 N. A. Bogoslovskiy and K. D. Tsendin, Physics of Switching and Memory Effects in Chalcogenide Glassy Semiconductors, *Semiconductors*, 2012, **46**, 559–590, DOI: 10.1134/S1063782612050065.

39 W. Wetnic and M. Wuttig, Reversible Switching in Phase-Change Materials, *Mater. Today*, 2008, 20–27, DOI: 10.1016/S1369-7021(08)70118-4.

40 P. Priyadarshini, P. C. Kumar and R. Naik, Tuning in Optoelectronic Properties of In/Te Bilayer Heterostructure upon Annealing at Different Temperatures: Surface Wettability and Photo Response Study for Photonic and Solar Cell Applications, *RSC Adv.*, 2024, **14**(18), 12897–12910, DOI: 10.1039/D4RA00807C.

41 W. Lan, J. Wang, Y. Fu and L. Cao, Room-Temperature near-Infrared Photodetectors Based on GeTe Film Grown by Pulsed Laser Deposition Method, *Thin Solid Films*, 2023, **775**, 139861, DOI: 10.1016/J.TSF.2023.139861.

42 P. Chinmay Kumar, S. Kanungo, P. Pradhan, S. Kumar Biswal, J. Kumar, C. Sripan and R. Naik, Tuning Hydrophilicity and Photoresponse by Interfacial Ag Diffusion in the Sb_2S_3 Layer for Optoelectronic Applications: An Experimental and Computational Study, *J. Phys. Chem. C*, 2024, **128**, 16740–16753, DOI: 10.1021/acs.jpcc.4c04263.

43 G. Konstantatos, J. Clifford, L. Levina and E. H. Sargent, Sensitive Solution-Processed Visible-Wavelength Photodetectors, *Nat. Photonics*, 2007, **1**, 531–534, DOI: 10.1038/nphoton.2007.147.